Inorganic Chemistry Communications 186 (2026) 116273

Contents lists available at ScienceDirect

Inorganic Chemistry Communications

journal homepage: www.elsevier.com/locate/inoche

Research Article

Biopolymer-stabilized selenium and selenium-copper nanoparticles with antioxidant and photoprotective dual functionality

Maria de Fatima C. da Silva Neta [a], Woodland de S. Oliveira [a], Ari S. Guimarães [a], Amanda G. da Veiga [b], Angel Perez-Roldan [c], Josue Carinhanha [a], Cintya D. Angeles do E.S. Barbosa [a], Jose L. Luque-Garcia [c,*], Daniela S. Anunciação [a,*]

[a] Instituto de Química e Biotecnologia, Universidade Federal de Alagoas, Campus A. C. Simões, 57072-900, Maceió, AL, Brazil.
[b] Instituto de Química, Universidade Federal do Rio de Janeiro, 21941-909, Rio de Janeiro, RJ, Brazil.
[c] Analytical Chemistry Department, Faculty of Chemical Sciences. Complutense University of Madrid, 28040 Madrid, Spain.

ARTICLE INFO

Keywords:
Selenium nanoparticles
Photoprotection
Antioxidant activity
Hybrid nanomaterials
Chitosan and PVA stabilization

ABSTRACT

The development of multifunctional nanomaterials with antioxidant and photoprotective properties offers significant potential for cosmetic and biomedical applications. In this study, selenium (SeNPs) and selenium–copper (SeCuNPs) nanoparticles were synthesized via chemical reduction using chitosan (CHI) and polyvinyl alcohol (PVA) as stabilizers. Transmission electron microscopy confirmed a spherical morphology, with mean sizes of 85.4 ± 20.2 nm (SeNPs_CHI) and 76.2 ± 12.0 nm (SeCuNPs_CHI), and significantly smaller sizes for PVA-stabilized formulations (34.3 ± 4.0 nm and 32.5 ± 5.8 nm, respectively). X-ray photoelectron spectroscopy (XPS) confirmed the presence of elemental selenium (Se^0) and copper (Cu^0) in the hybrid nanoparticles. All formulations exhibited potent antioxidant capacity, as demonstrated by $ABTS^{\bullet+}$, $DPPH^{\bullet}$, and FRAP assays, outperforming classical standards including Trolox®, ascorbic acid, and quercetin. In vitro sun protection factor (SPF) values were significantly higher than that of the commercial UV filter 2-hydroxy-4-methoxybenzophenone (BZF-3), particularly for SeCuNPs_PVA. Additionally, the nanoparticles displayed excellent photostability under simulated solar irradiation, maintaining or improving SPF over time. These findings highlight the potential of selenium-based nanoparticles, especially hybrid SeCuNPs, as multifunctional agents with strong antioxidant and photoprotective activity, offering a promising platform for the development of next-generation dermocosmetic and biotechnological products.

1. Introduction

In recent years, the deterioration of the ozone layer, primarily caused by the widespread use of chlorofluorocarbons (CFCs), has led to increased human exposure to ultraviolet (UV) radiation. This heightened exposure has intensified the search for effective strategies to protect cells from radiation-induced damage. Among these, antioxidants have gained significant attention due to their capacity to neutralize reactive oxygen species (ROS) generated by UV light, thereby reducing oxidative stress and cellular damage [1].

Nanotechnology has emerged as a promising tool for the development of advanced therapeutic and protective agents [2,3]. Among various nanomaterials, selenium nanoparticles (SeNPs) have garnered interest due to their lower toxicity compared to other selenium species [4] and their potent antioxidant properties [5]. These features enable SeNPs to serve as antitumor, anti-inflammatory, antimicrobial, and antidiabetic agents [6–12]. Beyond these therapeutic applications, SeNPs have demonstrated versatility in drug delivery systems, agriculture [13,14], nutritional supplementation [15], and food safety [16–20]. Despite this broad applicability, their use in dermocosmetic formulations remains underexplored, particularly their combined antioxidant and UV-protective potential under physiologically relevant exposure conditions.

To enhance the biological activity of selenium-based nanomaterials, the design of multielement systems has been proposed. Combining selenium with other redox-active elements in a single nanostructure may result in synergistic biological effects, improving ROS neutralization and expanding photoprotective properties via enhanced surface plasmon

* Corresponding authors.
E-mail addresses: jlluque@ucm.es (J.L. Luque-Garcia), daniela.anunciacao@iqb.ufal.br (D.S. Anunciação).

https://doi.org/10.1016/j.inoche.2026.116273
Received 28 September 2025; Received in revised form 24 January 2026; Accepted 29 January 2026
Available online 31 January 2026

resonance (SPR) [21,22].

In this context, metallic nanoparticles have attracted increasing attention in nanomedicine due to their unique physicochemical characteristics, including redox activity, high surface area, and the ability to interact with biological molecules. These properties support multifunctional roles in therapeutic, diagnostic, and protective applications. Nevertheless, challenges related to toxicity, biodistribution, and regulatory constraints must be addressed to ensure safe biomedical translation [23].

Among metallic elements, copper is of particular interest due to its essential biological role. Copper acts as a cofactor in key antioxidant enzymes such as copper/zinc-superoxide dismutase (SOD1), which catalyzes the dismutation of superoxide radicals and contributes to cellular redox homeostasis [24,25]. Copper-based nanoparticles have shown high catalytic efficiency and broad biological activity, including antimicrobial and anticancer effects [19,26–28]. Incorporating copper into selenium nanoparticles may therefore enhance antioxidant and photoprotective performance by integrating complementary redox pathways within a single nanostructure.

An additional key factor in optimizing the biomedical applicability of nanoparticles is surface functionalization. The use of stabilizing biopolymers such as chitosan and polyvinyl alcohol (PVA) enables control over particle size and colloidal stability while conferring biocompatibility, reduced toxicity, and functional groups capable of favorable biological interactions. These surface characteristics are critical in determining biological fate, cellular uptake, and overall efficacy in topical or systemic applications [29–31].

On this basis, the development of hybrid selenium–copper nanoparticles (SeCuNPs) and the comparative assessment of their antioxidant and photoprotective properties relative to SeNPs is of growing interest. However, current knowledge of SeCuNPs remains limited, particularly regarding their synthesis, physicochemical characterization, and functional evaluation in biomedical or topical contexts. Most studies to date have focused on optoelectronic [33,34], photocatalytic, or sensor-related applications [35–37], with limited attention to skin protection or dermocosmetic use.

In the cosmetic field, studies involving SeNPs remain scarce. One report described a SeNP-based topical formulation with promising UV-blocking activity [38], but the broader photoprotective potential of selenium-based nanomaterials—especially hybrid systems incorporating copper—remains largely unexplored.

Base don al lof the above, this study aimed to synthesize and characterize SeNPs and SeCuNPs stabilized with chitosan or PVA, and to evaluate their antioxidant capacity and in vitro photoprotective properties, including SPF determination and photostability under simulated solar exposure. The results contribute to advancing the understanding of multifunctional selenium-based nanomaterials and their applicability in the development of innovative cosmetic formulations for enhanced skin protection.

2. Materials and methods

2.1. Chemicals

All reagents used in this study were of analytical grade and ≥ 95% purity; no further purification was required. Solutions were prepared using ultrapure water (conductivity <0.1 μS/cm) obtained from a Mater System MS2000 purifier (GEHAKA, São Paulo, Brazil). The following chemicals were used: sodium selenite, polyvinyl alcohol (PVA), Trolox® (6-hydroxy-2,5,7,8-tetramethylchroman-2-carboxylic acid), sodium acetate, iron(III) chloride, chitosan, quercetin, benzophenone-3 (BZF-3; 2-hydroxy-4-methoxybenzophenone), DPPH• (1,1-diphenyl-2-picrylhydrazyl), potassium phosphate, potassium bromide, ABTS (2,2′-azino-bis (3-ethylbenzothiazoline-6-sulfonic acid)), and TPTZ (2,4,6-tripyridyl-*s*-triazine) from Sigma-Aldrich (Heidelberg, Germany), and potassium persulfate from Merck (Darmstadt, Germany). Copper(II) sulfate pentahydrate, glacial acetic acid, ascorbic acid, ethanol, and methanol were supplied by Synth (São Paulo, Brazil).

2.2. Synthesis of nanoparticles

Nanoparticles (NPs) were synthesized using a modified method based on a previous report [39]. For chitosan-stabilized NPs (SeNPs_CHI and SeCuNPs_CHI), solutions of 0.5% (*w/v*) chitosan (from shrimp shells, ≥ 75% deacetylated), 230 mmol/L ascorbic acid, 2.4 mol/L acetic acid, and 27 mmol/L sodium selenite were mixed in a 1:4:3:2 (*v*/v) ratio under constant stirring. For PVA-stabilized NPs (SeNPs_PVA and SeCuNPs_PVA), 50 mmol/L sodium selenite and 20 g/L PVA (Mw 31,000-50,000, 87–89% hydrolyzed) were mixed in a 1:1 (*v*/v) ratio, followed by addition of 100 mmol/L ascorbic acid in a 3:20 (v/v) ratio. The mixtures were stirred for 2 h at 25 °C [40]. To synthesized selenium-copper nanoparticles (SeCuNPs), Cu(II) sulfate solution (same concentration and volume as selenium precursor) was added. All nanoparticle suspensions were dialyzed for 8 h to remove excess ions and acidity, yielding a final pH of ~6.0.

2.3. Physicochemical characterization of nanoparticles

Nanoparticle morphology, size, and elemental composition were evaluated by transmission electron microscopy (TEM) and energy-dispersive X-ray spectrometry (EDX) using a JEM 3000F high-resolution microscope (JEOL, Peabody, MA, USA) equipped with an INCA Energy+ microanalysis system (Oxford Instruments, Concord, MA, USA). SeNPs and SeCuNPs were mounted on carbon-coated copper or nickel grids, respectively. Particle size (n = 150) was calculated from TEM images using ImageJ (v1.46r, Java).

X-ray photoelectron spectroscopy (XPS) was performed on lyophilized SeCuNPs_CHI using a Thermo Scientific ESCALAB 250Xi spectrometer (Thermo Fisher Scientific, Waltham, MA, USA) under ultra-high vacuum (<5×10^{-9} bar), with Al Kα radiation (1486.6 eV). The Au 4f7/2 line (84.0 eV) was used for binding energy calibration. Survey spectra were acquired at 100 eV pass energy, while high-resolution Cu2p and Se3d spectra were recorded at 25 eV. Data analysis and curve fitting (Gaussian-Lorentzian) were performed with Thermo Avantage© software.

Hydrodynamic radii were measured using a Zetatrac NPA 152–31 particle size analyzer (Microtrac, Montgomeryville, PA, USA). Functional groups were assessed by Fourier-transform infrared (FTIR) spectroscopy (Nicolet IR 200, Thermo Scientific) using KBr pellets, recorded between 4000 and 400 cm^{-1} at 4 cm^{-1} resolution. UV–Vis absorption spectra were acquired from 200 to 1100 nm using an AJX-6100PC spectrophotometer (Micronal, São Paulo, Brazil).

2.4. Antioxidant activity assays

$ABTS^{\bullet+}$ was prepared by reacting 5 mmol/L ABTS (2,2′-aziobis(3-ethylbenzothiazoline-6-sulfonate) with potassium persulfate (6:1 M ratio) and incubating the mixture in the dark for 16 h. The solution was diluted with 0.05 mol/L phosphate buffer (pH 7.4 ± 0.1) to a final volume of 25 mL. In the assay, 88 μL of $ABTS^{\bullet+}$ was added to the standard or sample solution and made up to 2.0 mL with deionized water. Absorbance was measured at 734 nm after 15 min [41].

For the $DPPH^{\bullet}$ assay, to 100 μL of 600 μmol/L $DPPH^{\bullet}$ in methanol, the standard or sample solution was added and the volume adjusted to 2.0 mL with 30% (*v*/v) ethanol. Absorbance was measured at 527 nm after 30 min. NP concentrations ranged from 0.05 to 0.8 μg/L, and standard concentrations from 0.1 to 3.0 μg/L [42]. The percentage of inhibition (%*I*) was calculated using the eq. (1):

$$\%I = \left(1 - \left(A_{AO}/A_{ref}\right)\right) \times 100 \quad (1)$$

where A_{AO} is the absorbance of the antioxidant sample and A_{ref} is the

absorbance of the blank.

The FRAP reagent was composed of 10 mmol/L $FeCl_3$, 20 mmol/L TPTZ, and 0.3 mol/L acetate buffer (pH 3.6). A volume of 400 μL of reagent and a suitable volume of standard or sample were mixed and diluted to 2.0 mL with ultrapure water. Absorbance was measured at 593 nm after 10 min. NP concentrations ranged from 1.0 to 4.0 μg/mL; standads ranged from 0.25 to 10 μg/mL. Each curve was constructed in triplicate with at least six data points. Results were expressed according to the sensitivity of the analytical curves (A_{593} μg / L).

2.5. In vitro Sun protection factor (SPF)

SPF was determined for the NPs and BZF-3 by scanning absorbance from 280 to 400 nm. The absorbance at 290 nm (λ_{max} of BZF-3) was used to construct calibration curves. Measurements were performed in triplicate at 15 and 25 μg/L. SPF values were calculated using the Mansur eq. (2) (Mansur et al., 1986):

$$SPF = CF \times \Sigma EE_{(\lambda)} \times I_{(\lambda)} \times A_{(\lambda)} \quad (2)$$

where CF is a correction factor equal to 10 (SPF 4 in 8% homosalate (m/m)); $EE_{(\lambda)}$ is the erythematogenic effect of radiation at wavelength λ; $I_{(\lambda)}$ is the solar intensity, and $A_{(\lambda)}$ is the sample absorbance at wavelength (λ).

2.6. Photostability assay

Photostability was evaluated based on modified protocols [43,44]. NP suspensions (5 mL) at 15 and 25 μg/mL were placed in Petri dishes and irradiated under a solar simulator equipped with UVA (320–400 nm) and UVB (280–320 nm) lamps (30 W). Samples were exposed for up to 120 min and analyzed by UV–Vis spectroscopy from 280 to 400 nm. SPF values were recalculated after each time point using the Mansur method [45].

2.7. Statistical analysis

All data were expressed as mean ± standard deviation (SD) based on triplicate measurements ($n = 3$), except where otherwise noted. Statistical analysis was performed using Student's *t*-test ($p < 0.05$) and one-way ANOVA followed by Tukey's post hoc test ($\alpha = 0.05$). Statistical evaluations were conducted using OriginPro 9.0 software (OriginLab, Northampton, MA, USA).

3. Results and discussion

3.1. Characterization of nanoparticles

High-resolution transmission electron microscopy (HR-TEM) revealed that all NPs exhibited a predominantly spherical morphology with narrow size distributions (Fig. 1A). The average diameters were 85 ± 20 nm and 76 ± 12 nm for SeNPs stabilized with chitosan (SeNPs-CHI) and polyvinyl alcohol (SeNPs_PVA), respectively. For the selenium-copper hybrid nanoparticles (SeCuNPs), the sizes were significantly smaller: 34 ± 4 nm (SeCuNPs_CHI) and 32.5 ± 6 nm (SeCuNPs-PVA). These results suggest that particle size was not substantially influenced by the type of stabilizer, but rather by the elemental composition.

The average particle sizes observed for SeNPs are in good agreement with previous reports [46,47]. The role of polymeric stabilizers such as chitosan and PVA is critical in modulating particle size, primarily by controlling nucleation and inhibiting growth and agglomeration during synthesis. The smaller size of SeCuNPs compated to SeNPs is consistent with literature reports on hybrid metal nanoparticles, where incorporation of a second metal (e.g., Cu, Mg, Fe, Ni) tends to reduce particle diameter due to modified crystallization kinetics or lattice distortion [48–53].

Dynamic light scattering (DLS) measurements confirmed the trends observed in HR-TEM (Fig. 1B). SeNPs_CHI and SeNPs_PVA exhibited hydrodynamic diameters of 125 ± 26 and 98 ± 13 nm, respectively. SeCuNPs showed smaller hydrodynamic diameters: 71 ± 20 nm (SeCuNPs_CHI) and 70 ± 12 nm (SeCuNPs_PVA). As expected, DLS values were larger than HR-TEM measurements due to the hydration shell and surface-bond molecules present in aqueous dispersions.

Energy-dispersive X-ray spectroscopy (EDX) confirmed the elemental composition of the NPs (Fig. 1C). SeNPs exhibited distinct selenium signals [54,55], while SeCuNPs displayed both Se and Cu peaks [56–58] in a 1:1 M ratio. Minor signals of C and O signals were attributed to residual stabilizing agents, while Ni and Fe peaks originated from the TEM grids and equipment. Elemental mapping (Fig. 1D), revealed homogenous distribution of Se and Cu throughout the SeCuNPs, consistent with the formation of well-integrated hybrid nanostructures.

X-ray photoelectron spectroscopy (XPS) was performed to investigate the chemical states of Se and Cu. Survey spectra confirmed the presence of Se, Cu, C, O and N (Supporting Information Fig. S1A and Table S1), with C, O, and N corresponding to the chitosan matrix. The 1:1 stoichiometric ratio of Se and Cu was in line with the results provided by the EDX analysis. High-resolution Se3d and Cu2p spectra were taken to evaluate the Se and Cu chemical species in the SeCuNPs. The level line of the Cu2p nucleus (Supporting Information Fig. S1B) showed a binding energy of 932.4 eV, which may correspond to Cu^0 or Cu(I). The Auger CuLMM line was analyzed to confirm the oxidation state, which has a different shape and kinetic energy for each species [59]. The CuLMM line spectrum for the nanomaterial (Supporting Information Fig. S1C) is compatible with Cu^0. The spectrum of the Se3d lump level (Supporting Information Fig. S1D) shows a doublet at 54.1 and 54.9 eV, referring to the Se^0 species.

UV–Vis molecular absorption spectroscopy revealed that SeNPs exhibited a characteristic intense orange color with absorption maxima at 260 nm (SeNPs_CHI) and 258 nm (SeNPs_PVA), associated with their surface plasmon resonance (SPR) (Fig. 1E). These values are in accordance with literature data [60–65]. SeCuNPs displayed two absorption bands: one near 250 nm (similar to SeNPs), and another at 896 nm (SeCuNPs_CHI) or 918 nm (SeCuNPs_PVA) (Fig. 1E), consistent with previous reports of Cu—Se hybrid system [36,66]. These dual-band profiles support the successful formation of bimetallic nanoparticles.

The wavelengths of maximum absorption (λ_{max}) obtained for the SeNPs agree with literature data, where maximum absorption is reported from 260 to 268 nm [4,54,55,65,67,68]. These absorption wavelengths correspond to the surface plasmon resonance (SPR) of these materials, which can undergo shifts depending on factors such as particle size, shape and composition, as well as the environment in which they are present [63,67,69]. The SeCuNPs hybrid nanoparticles exhibit a distinct absorption profile, with two absorption bands. The first, observed at around 250 nm, is compatible with that of pure SeNPs, with a slight shift of up to 10 nm. The second band, with a λ_{max} at approximately 1000 nm, corroborates what is observed for nanomaterials containing selenium and copper [33,34,70].

Fourier-transform infrared (FTIR) spectra confirmed the presence of stabilizing agents on the NP surfaces and revealed interactions between groups and the nanomaterials (Fig. 1F). SeNPs-CHI and SeCuNPs_CHI displayed N—H stretching bands near 3719–3711 cm^{-1} and O—H stretching bands between 3433 and 3464 cm^{-1}, slightly shifted from native chitosan (3736 and 3410 cm^{-1}). Similar shifts were observed for PVA-stabilized NPs: O—H stretching bands at 3418 cm^{-1} (NPs) versus 3426 cm^{-1} (PVA), and methylene C—H deformation bands at 1620–1597 cm^{-1}. These spectral shifts suggest hydrogen bonding or electrostatic interactions between polymer hydroxyl/amine groups and the NP surfaces, consistent with previous findings [54,71,72].

Comparing the spectra of CHI and SeNPs_CHI and SeCuNPs_CHI, it is possible to see shifts in the O—H bands from 3750 to 3730 cm^{-1}. Similarly, SeNPs_PVA and SeCuNPs_PVA showed shifts in the O—H

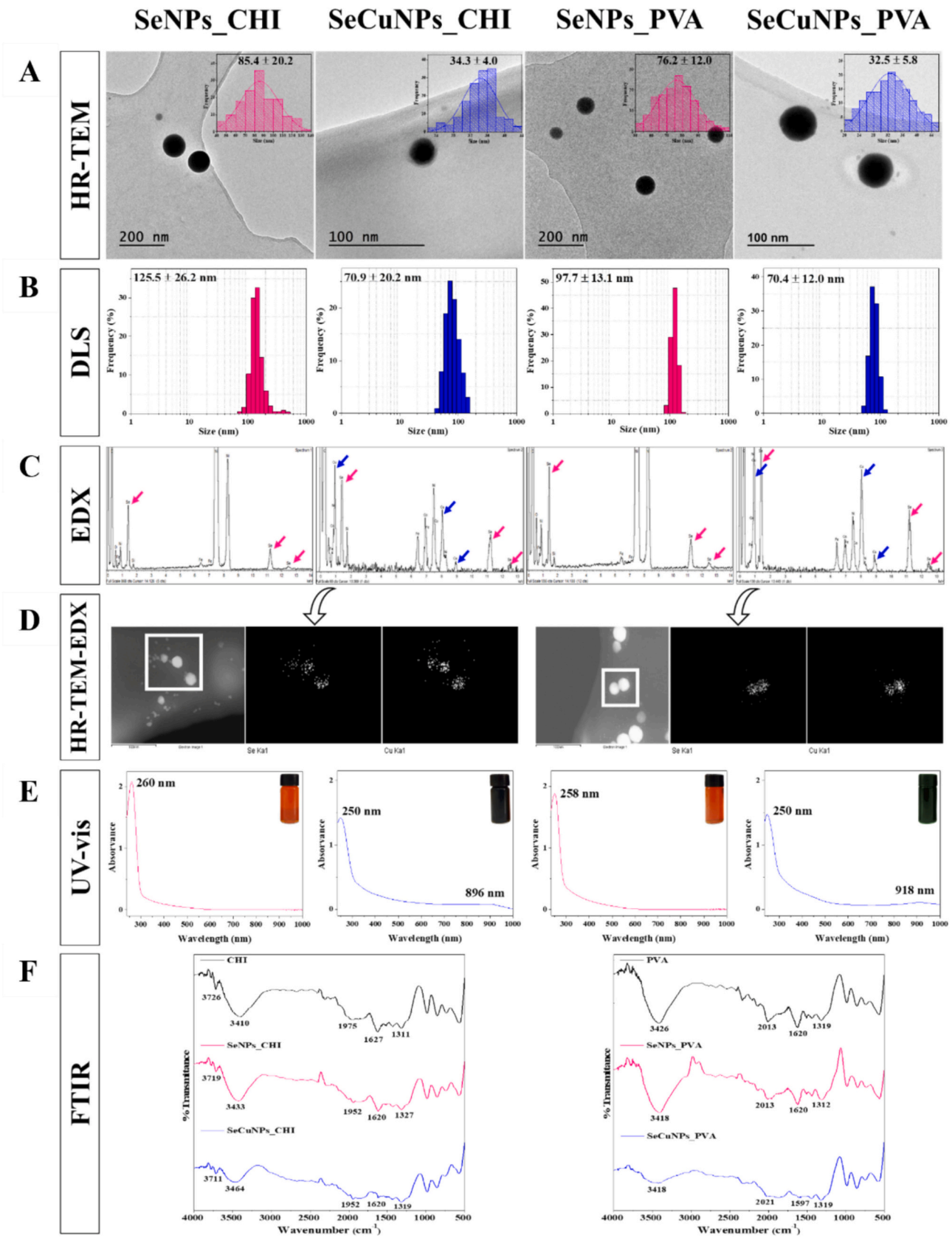

Fig. 1. Physicochemical characterization of the synthesized nanoparticles (NPs). (A) High-resolution transmission electron microscopy (HR-TEM) images showing morphology and size distribution. (B) Dynamic light scattering (DLS) histograms indicating hydrodynamic size. (C) Energy-dispersive X-ray spectroscopy (EDX) spectra confirming elemental composition; selenium (Se) peaks marked with pink arrows, copper (Cu) peaks with blue arrows. (D) Elemental mapping of Se and Cu in SeCuNPs by HR-TEM/EDX, showing uniform spatial distribution. (E) UV–visible absorption spectra of SeNPs and SeCuNPs stabilized with chitosan and PVA. (F) Fourier-transform infrared (FTIR) spectra showing characteristic functional groups and surface interactions with stabilizers.

bands compared to PVA, from 3750 to 3730 and 3720 cm^{-1}, respectively. Such shifts are reported by several authors and suggest an interaction between the O—H groups of the stabilizers and the surface of the NPs, highlighting the importance of these groups for stabilization and dispersion of NPs [46,54,61,67,73,74].

Overall, the data confirm the successful synthesis of monometallic (SeNPs) and bimetallic (SeCuNPs) nanoparticles with well-defined size, composition, and surface functionality, stabilized by biocompatible polymers. These physicochemical characteristics support their further evaluation in antioxidant and photoprotective applications.

3.2. Antioxidant activity of SeNPs and SeCuNPs

The antioxidant capacity (AOC) of SeNPs and SeCuNPs was evaluated using three complementary assays: $ABTS^{\bullet+}$ and $DPPH^{\bullet}$ radical scavenging methods, and the ferric reducing antioxidant power (FRAP) assay. Results were compared to well-known antioxidants of varying polarity and mechanisms of action: ascorbic acid, quercetin and Trolox®.

In the $ABTS^{\bullet+}$ assay (Fig. 2A), all nanoparticles exhibited excellent radical scavenging activity, with half-maximal inhibitory concentration (IC_{50}) values ranging from 0.28 ± 0.03 to 0.30 ± 0.01 μg/mL. These values were statistically comparable to quercetin (IC_{50} = 0.33 ± 0.01 μg/ mL; ANOVA with Tukey post hoc, $p < 0.05$) and significantly more potent, by 81 and 86%, than ascorbic acid and Trolox®, respectively. These findings surpass those reported in previous studies using similarly sized SeNPs, which achieved values near 2.7 μg/mL [75] or 40% inhibition at 1 mmol/L [54].

In the $DPPH^{\bullet}$ assay, a similar antioxidant trend was observed (Fig. 2A). Nanoparticles stabilized with chitosan showed the strongest activity, particularly SeNPs_CHI (IC_{50} = 0.27 ± 0.02 μg/mL) and SeCuNPs_CHI (IC_{50} = 0.37 ± 0.03 μg/mL), outperforming quercetin (IC_{50} = 2.04 ± 0.02 μg/ mL), the most effective standard against the radical, by 82–87%. PVA-stabilized nanoparticles also showed potent activity, although with slightly higher IC_{50} values, still 73–75% lower than the standard. These results are associated with the high AOC of SeNPs previously described [54,63,67,76], and suggest that the antioxidant performance is influenced not only by the nanoparticle composition, but also by surface chemistry and stabilizer type. The superior efficacy of CHI-based nanoparticles may stem from synergistic effects between the Se core and the functional groups of chitosan, such as amino and hydroxyl groups, which are known to participate in radical scavenging [77].

The strong radical-scavenging performance of the NPs in both the $ABTS^{\bullet+}$ and $DPPH^{\bullet}$ assays implies that their antioxidant mechanisms likely involve both electron transfer (ET) and hydrogen atom transfer (HAT) processes. Chitosan with a high degree of deacetylation and lower molecular weight has been shown to enhance antioxidant properties by increasing the accessibility of amino groups and solubility [77], which align our observations for CHI-stabilized NPs.

In the FRAP assay, all NPs demonstrated marked ferric reducing power relative to the standards (Fig. 2A). SeNPs, irrespective of stabilizer, showed 2.8–8.5-fold greater reducing capacity than quercetin and Trolox®. Among the hybrid NPs, SeCuNPs_PVA exhibited the highest FRAP activity, with sensitivity values 2.1-fold and 6.4-fold higher than quercetin and Trolox®, respectively. The ability to reduce Fe(III) to Fe (II) further supports the involvement of ET mechanisms in antioxidant action.

To rule out the influence of precursor compounds, control experiments were conducted with chitosan, PVA, and Se(IV) precursors at 50 μg/mL. These exhibited negligible AOC (<10%) across all methods, confirmed that the observed antioxidant effects are intrinsic to the synthesized SeNPs and SeCuNPs.

Overall, the results demonstrate that both SeNPs and SeCuNPs possess remarkable antioxidant capacity, exceeding that of classical antioxidant standards. These findings are consistent with the known biological activity of selenium, including the modulation of redox enzymes such as glutathione peroxidase (GPx), thioredoxin reductases (TRs), and iodothyronine deiodinases (DIO) [63,78–80].

The superior antioxidant and photoprotective performance observed for SeCuNPs compared to SeNPs may be attributed both to differences in physicochemical characteristics of the nanoparticles and to a synergistic interaction between selenium and copper at the nanoscale. On one hand, key parameters such as particle size, shape, agglomeration state,

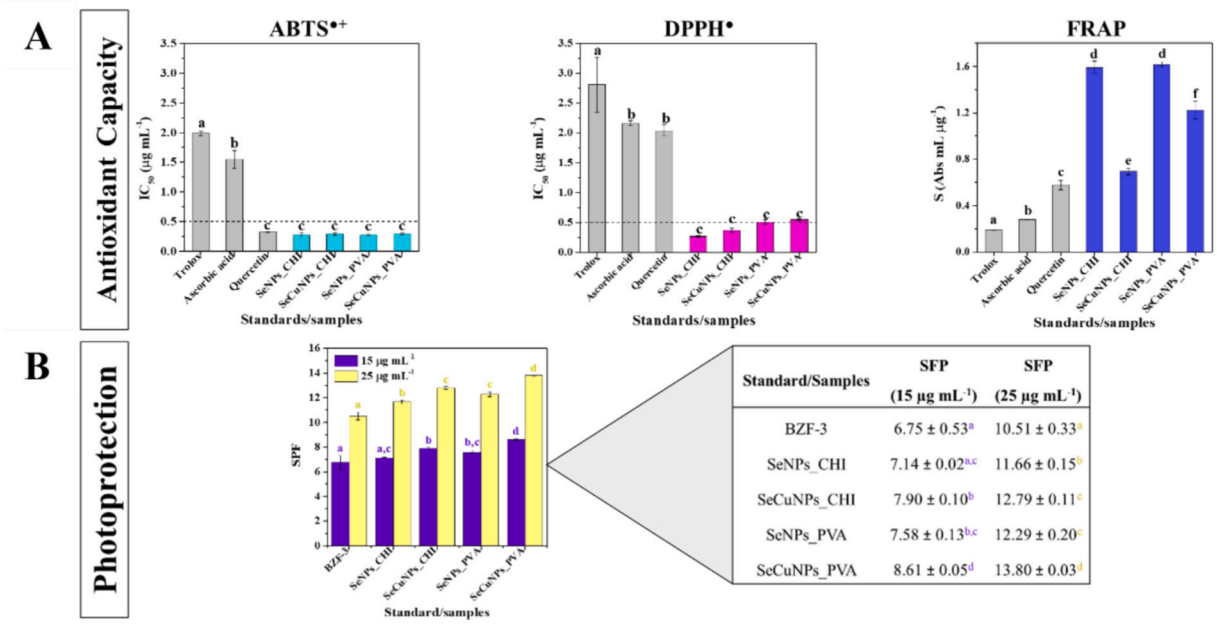

Fig. 2. (A) Antioxidant activity of SeNPs and SeCuNPs evaluated by $ABTS^{\bullet+}$ and $DPPH^{\bullet}$ radical scavenging assays (expressed as IC_{50} values), and the ferric reducing antioxidant power (FRAP) assay (expressed as sensitivity values). (B) In vitro sun protection factor (SPF) values of BZF-3 (reference compound) and synthesized nanoparticles at 15 and 25 μg/mL. Data represent mean ± SD (n = 3). Statistical analysis was performed by one-way ANOVA followed by Tukey's post hoc test ($p < 0.05$). Different letters indicate statistically significant differences among groups.

chemical composition, surface charge, and surface functionalization strongly influence biological interactions, redox activity, dispersion stability, and potential adverse effects. Accordingly, the differences observed between SeNPs and SeCuNPs, as well as between chitosan- and PVA-stabilized systems, can be partially explained by variations in these parameters. In particular, reduced particle size, hybrid composition, and polymer-mediated surface interactions may enhance contact with reactive oxygen species and facilitate electron-transfer processes [81]. These results align with previous findings demonstrating that engineered nanomaterials can modulate oxidative stress through redox-related pathways, with surface properties playing a pivotal role in cellular response and ROS scavenging [82]. On the other hand, the observed synergy may also be attributed to the complementary redox properties of both elements. Selenium plays a key role in the catalytic cycle of antioxidant enzymes such as glutathione peroxidase (GPx), while copper is an essential cofactor in superoxide dismutase (SOD1), which catalyzes the dismutation of superoxide radicals [64,79,80]. The coexistence of Se and Cu on the nanoparticle surface may provide a broader redox-active interface, allowing more effective neutralization of diverse reactive oxygen species (ROS). In addition, the hybrid composition may enhance light absorption through dual-band surface plasmon resonance, as observed in the UV–Vis spectra, which could contribute to the improved photoprotective properties [36,70]. Although the exact molecular mechanism of this synergy remains to be fully elucidated, these findings indicate that the combination of selenium and copper within a single nanostructure can significantly potentiate its biological functions. Further mechanistic studies, including redox cycling assays and enzymatic activity analyses, will be required to clarify the precise interactions responsible for these effects.

3.3. *In vitro Sun protection factor (SPF)*

The sun protection factor (SPF) of the synthesized NPs was assessed spectrophotometrically using an in vitro method previously described [45]. Preliminary UV–Vis absorption scans confirmed that all NPs exhibited significant absorbance in both the UVA (320–400 nm) and UVB regions (290–320 nm). The absorbance at 290 nm was used to establish the linearity range, which was found to be between 1 and 30 μg/mL for all nanoparticle formulations (Supporting Information Fig. S2).

Based on this linearity, SPF values were calculated at concentrations of 15 and 25 μg/mL for each NP formulation and compared to the standard compound benzophenone-3 (BZF-3). The synthesized NPs showed SPF values in the range of 7.14 to 11.66 (SeNPs_CHI), 7.90 to 12.79 (SeCuNPs_CHI), 7.58 to 12.29 (SeNPs_PVA) and 8.61 to 13.80 (SeCuNPs_PVA), for 15 and 25 μg/mL, respectively (Fig. 2B).

All synthesized NPs demonstrated higher SPF values than BZF-3 reference compound at equivalent concentrations. Notably, SeCuNPs_PVA showed the highest SPF, nearly doubling the protection offered by BZF-3 at 25 μg/mL. The SPF values achieved exceeded the minimum threshold (SPF $\geq$ 6) established by the Brazilian regulatory agency ANVISA [83], indicating their potential suitability as active protective agents.

Statistical analysis (one-way ANOVA followed by Tukey's post hoc test, $p < 0.05$) confirmed significant differences in SPF performance among the tested formulations, particularly favoring the SeCuNPs_PVA (Fig. 2B).

The photoprotective performance of the nanoparticles is closely related to their optical properties. The UV–Vis spectra revealed that SeNPs exhibited a single absorption band in the UVB region (~258–260 nm), while SeCuNPs presented **dual absorption bands**, with one peak around 250 nm and a second, broader peak in the near-infrared region (~896–918 nm), which aligns with UVA absorbance and is characteristic of surface plasmon resonance (SPR) phenomena [36,70]. This dual-band behavior supports a mechanism based on **broad-spectrum UV absorption**, rather than light scattering. Given that the nanoparticles have sizes well below 100 nm, **Rayleigh scattering is expected to be minimal**, and the observed SPF values are likely driven by true photon absorption. The improved photoprotective capacity of SeCuNPs can thus be attributed to their enhanced electronic structure and SPR properties, which enable efficient absorption in both the UVA and UVB regions. These findings reinforce the potential of SeCuNPs as next-generation UV-absorbing agents.

Although protoprotective studies have predominantly focused on titanium dioxide and zinc oxide nanoparticles, currently approved as inorganic UV filters in sunscreens [84,85], selenium-based nanomaterials remain underexplored in this field. However, emerging evidence suggests their promise. For instance, a topical formulation containing SeNPs (200 mg) stabilized with sodium lauryl sulfate solution (4% *w/v*) and probiotic ingredients achieved an SPF of 29.77 [38], supporting the relevance of this approach.

The results presented here demonstrate that SeNPs and SeCuNPs not only exhibit strong antioxidant activity but also significant UV-block capabilities, indicating their potential use as multifunctional components in sunscreen or dermocosmetic formulations.

These results suggest that the observed dual functionality may occur at distinct skin compartments. The photoprotective effect is likely confined to the stratum corneum, where the nanoparticles can efficiently absorb UV radiation, while the antioxidant activity would require interaction with the viable epidermis, where ROS generation takes place. Although the current study did not assess skin penetration, the particle size and surface properties of the NPs suggest a limited but possible interaction with upper viable layers, as described for other metal-based systems. Future studies will be needed to confirm this, including permeation, cytotoxicity, and biocompatibility analyses in skin models to ensure efficacy and safety for topical applications.

3.4. *In vitro Photostability study*

Photostability refers to the ability of a substance to retain its structural and functional integrity upon exposure to solar radiation, and it is a critical parameter in ensuring the safety and efficacy of sunscreen formulations. A lack of photostability can reduce photoprotective performance and potentially lead to adverse dermatological effects, including photoallergy and phototoxicity, due to the formation of degradation byproducts in the skin [86,87].

The photostability of SeNPs and SeCuNPs was evaluated over a 2 h exposure period, reflecting the recommended sunscreen reapplication interval [88]. UV–Vis absorption spectra revealed that all nanoparticle formulations exhibited an increase in absorbance following UV exposure (Fig. 3). At a fixed wavelenght of 300 nm, the absorbance of SeNPs-CHI increased by 21% at both tested concentrations (15 and 25 μg/mL). SeNPs_PVA showed slightly lower increases of 13% and 9%, respectively. The hybrid SeCuNPs_CHI formulation exhibited absorbance increases from 14 to 20%, whereas SeCuNPs_PVA showed mmore moderate changes, increasing from 14 to 16% with rising concentration.

These findings demonstrate good photostability across all formulations, with absorbance values retained at approximately 80% or higher throughout the 2 h irradiation period. The observed increases in absorption may be attributable to slight changes in nanoparticle size distribution induced by prolonged irradiation, as reported by Gubitosa et al. [43] in studies involving ellagic acid-coated gold nanoparticles stabilized with chitosan. Similar post-irradiation effects have been noted in commercial UV filters and formulations, where shifts in absorbance or degradation necessitate the inclusion of stabilizing agents such as octocrylene or bemotrizinol for compounds like avobenzone [87,89–91].

To better quantify photoprotective stability, SPF values were calculated at multiple irradiation time points for each NP formulation and concentration. As shown in Table 1, SPF values increased progressively over the exposure period, particularly for chitosan-stabilized NPs, where variations ranged from 17% to 24%, compared to 11% to 15% for PVA-

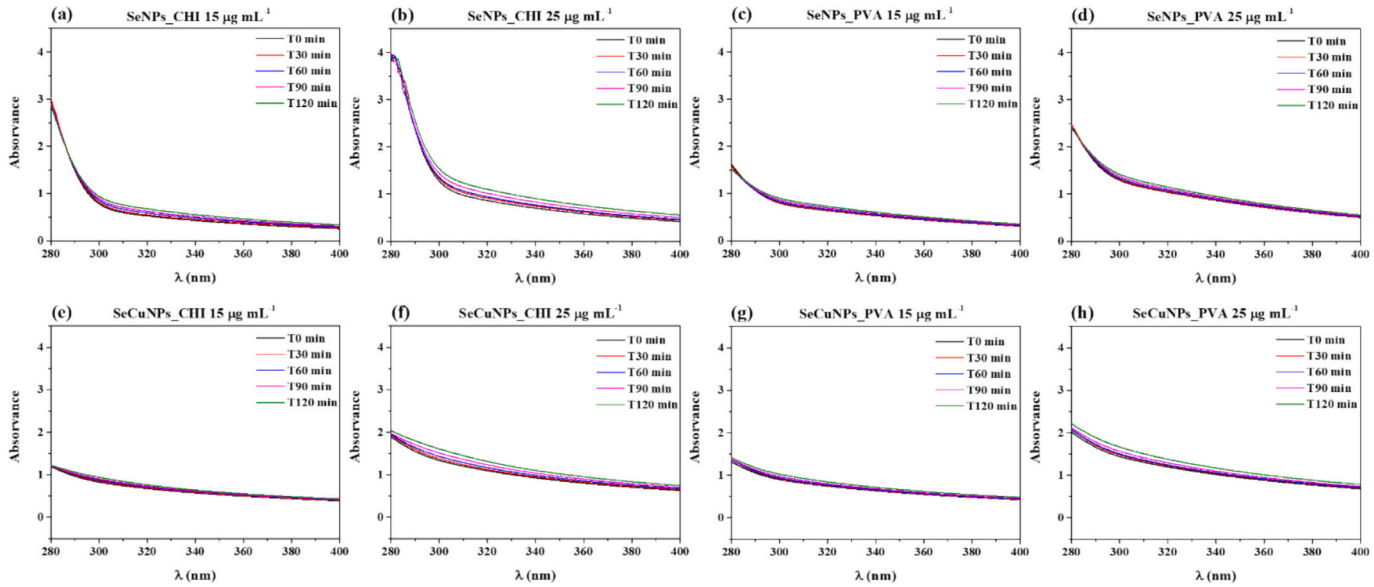

Fig. 3. UV–Vis absorption spectra of SeNPs and SeCuNPs recorded at different irradiation times (T_0 min to T_{120} min) under simulated solar exposure. (a) SeNPs_CHI at 15 μg/mL; (b) SeNPs_CHI at 25 μg/mL; (c) SeNPs_PVA at 15 μg/mL; (d) SeNPs_PVA at 25 μg/mL; (e) SeCuNPs_CHI at 15 μg/mL; (f) SeCuNPs_CHI at 25 μg/mL; (g) SeCuNPs_PVA at 15 μg/mL; (h) SeCuNPs_PVA at 25 μg/mL.

Table 1
In vitro sun protection factor (SPF) values of SeNPs and SeCuNPs at concentrations of 15 and 25 μg/mL, measured after 0, 30, 60, 90, and 120 min of UV irradiation. SPF values were calculated using the Mansur method based on UV absorbance measurements. Data represent mean ± SD ($n = 3$).

Time (min)	SPF (UVA and UVB radiation)							
	SeNPs_CHI		SeNPs_PVA		SeCuNPs_CHI		SeCuNPs_PVA	
	15 μg/mL	25 μg/mL	15 μg/mL	25 μg/mL	15 μg/mL	25 μg/mL	15 μg/mL	25 μg/mL
T0	7.14 ± 0.02	11.66 ± 0.15	7.58 ± 0.13	12.29 ± 0.20	7.90 ± 0.10	12.79 ± 0.11	8.61 ± 0.05	13.80 ± 0.03
T30	7.51 ± 0.07	12.24 ± 0.04	7.75 ± 0.06	12.46 ± 0.04	8.16 ± 0.04	13.19 ± 0.02	8.83 ± 0.06	14.24 ± 0.08
T60	7.95 ± 0.08	12.59 ± 0.07	7.98 ± 0.08	12.76 ± 0.05	8.48 ± 0.10	13.69 ± 0.04	8.98 ± 0.10	14.43 ± 0.06
T90	8.38 ± 0.14	13.31 ± 0.03	8.32 ± 0.10	13.14 ± 0.06	8.76 ± 0.18	14.37 ± 0.10	9.28 ± 0.11	14.86 ± 0.15
T120	8.83 ± 0.49	14.26 ± 0.09	8.75 ± 0.15	13.59 ± 0.11	9.27 ± 0.32	15.23 ± 0.15	9.76 ± 0.18	15.62 ± 0.33

stabilized NPs. These data suggest slightly greater photostability for PVA-based formulations, despite the higher initial SPF values of CHI-stabilized NPs.

Overall, the photostability profiles of SeNPs and SeCuNPs reinforce their suitability as multifunctional components in topical photoprotective systems, combining strong UV absorption with structural resilience under irradiation.

4. Conclusions

This study demonstrated that selenium-based nanoparticles (SeNPs) and selenium–copper hybrid nanoparticles (SeCuNPs), stabilized with chitosan or polyvinyl alcohol, possess robust multifunctional properties with direct relevance for biotechnological and dermocosmetic applications. The nanoparticles exhibited remarkable antioxidant activity, with IC_{50} values significantly superior to classical standards, and operated via mechanisms involving both electron and hydrogen atom transfer. In parallel, all formulations showed enhanced photoprotective performance, with SPF values exceeding those of the commercial reference compound BZF-3, especially for the SeCuNPs_PVA formulation.

Importantly, the nanoparticles also displayed notable photostability under simulated UV irradiation, a critical attribute for the development of durable and safe topical products. The combined antioxidant and photoprotective effects position these nanomaterials as promising multifunctional platforms for use in next-generation sunscreen formulations or dermoprotective agents.

This work represents an initial proof-of-concept, and further investigations are required to support translational applications. In particular, future studies will be focused on in vitro and **in vivo validation**, including preclinical safety and efficacy assessments using animal models or reconstructed skin systems, to confirm biological compatibility, protective performance, and long-term safety under physiological conditions. Addressing these aspects will be essential for advancing selenium- and selenium–copper-based nanoparticles toward practical cosmetic and biomedical use.

CRediT authorship contribution statement

Maria de Fatima C. da Silva Neta: Writing – original draft, Methodology, Investigation. **Woodland de S. Oliveira:** Methodology, Investigation. **Ari S. Guimarães:** Writing – original draft, Methodology, Investigation. **Amanda G. da Veiga:** Writing – original draft, Methodology, Investigation, Conceptualization. **Angel Perez-Roldan:** Writing – original draft, Methodology, Investigation. **Josue Carinhanha:** Writing – review & editing, Formal analysis, Data curation, Conceptualization. **Cintya D. Angeles do E.S. Barbosa:** Writing – review & editing, Supervision, Formal analysis, Data curation, Conceptualization. **Jose L. Luque-Garcia:** Writing – review & editing, Supervision, Resources, Project administration, Funding acquisition, Formal analysis, Data curation, Conceptualization. **Daniela S. Anunciação:** Writing – review & editing, Validation, Supervision, Project administration, Formal analysis, Data curation, Conceptualization.

Declaration of competing interest

The authors declare that they have no known competing financial interests or personal relationships that could have appeared to influence the work reported in this paper.

Acknowledgements

The authors acknowledge the financial support and infrastructure provided by CAPES, FAPEAL, CNPq, FINEP, and the Institute of Chemistry and Biotechnology of UFAL. J.L.L.G. acknowledge financial support by the Ministry of Science, Innovation and Universities (grant number: PID2023-150182OB-I00). M.F.C.S.N. acknowledges the FAPEAL scholarship (Process No. E:60030.0000000156/2022). The authors also thank Professor Maria Luiza Rocco for her valuable support with the XPS data and the Multiuser X-Ray Photoelectron Spectroscopy Laboratory at the Institute of Chemistry – UFRJ for performing the XPS analyses.

Appendix A. Supplementary data

Supplementary data to this article can be found online at https://doi.org/10.1016/j.inoche.2026.116273.

Data availability

Data will be made available on request.

References

[1] C. Caddeo, K. Teskač, C. Sinico, J. Kristl, Effect of resveratrol incorporated in liposomes on proliferation and UV-B protection of cells, Int. J. Pharm. 363 (2008) 183–191, https://doi.org/10.1016/j.ijpharm.2008.07.024.

[2] Z. Li, H. Zhang, Q. Gong, K. Luo, Biomaterials nanoplatform-based tumor vaccines for immunotherapy, Bioact. Mater. 51 (2025) 924–961, https://doi.org/10.1016/j.bioactmat.2025.06.038.

[3] G. Liu, B. Wang, P. Chen, Z. Liz, X. Cheng, Q. Gong, K. Luo, Redox-responsive dendritic copolymer–drug conjugates enhance therapeutic mitophagy through coordinated microtubule destabilization for synergistic triple-negative breast cancer therapy, Acta Biomater. (2025), https://doi.org/10.1016/j.actbio.2025.06.038. Online ahead of print.

[4] J. Zhou, D. Zhang, X. Lv, X. Liu, W. Xu, L. Chen, J. Cai, Z. Din, S. Cheng, Green synthesis of robust selenium nanoparticles via polysaccharide–polyphenol interaction: design principles and structure–bioactivity relationship, ACS Sustain. Chem. Eng. 10 (2022) 2052–2062, https://doi.org/10.1021/acssuschemeng.1c06048.

[5] A. Khurana, S. Tekula, M.A. Saifi, P. Venkatesh, C. Godugu, Therapeutic applications of selenium nanoparticles, Biomed. Pharmacother. 111 (2019) 802–812, https://doi.org/10.1016/j.biopha.2018.12.146.

[6] K. Bai, B. Hong, J. He, Z. Hong, R. Tan, Preparation and antioxidant properties of selenium nanoparticles-loaded chitosan microspheres, Int. J. Nanomedicine 12 (2017) 4527–4539, https://doi.org/10.2147/IJN.S129958.

[7] Y. Wang, J. Wang, H. Hao, M. Cai, S. Wang, J. Ma, Y. Li, C. Mao, S. Zhang, In vitro and in vivo mechanism of bone tumor inhibition by selenium-doped bone mineral nanoparticles, ACS Nano 10 (2016) 9927–9937, https://doi.org/10.1021/acsnano.6b03835.

[8] C. Zhu, S. Zhang, C. Song, Y. Zhang, Q. Ling, P.R. Hoffmann, J. Li, T. Chen, W. Zheng, Z. Huang, Selenium nanoparticles decorated with *Ulva lactuca* polysaccharide potentially attenuate colitis by inhibiting NF-κB mediated hyper-inflammation, J. Nanobiotechnol. 15 (2017) 20, https://doi.org/10.1186/s12951-017-0252-y.

[9] S. Zeng, Y. Ke, Y. Liu, Y. Shen, L. Zhang, C. Li, A. Liu, L. Shen, X. Hu, H. Wu, W. Wu, Y. Liu, Synthesis and antidiabetic properties of chitosan-stabilized selenium nanoparticles, Colloids Surf. B. Biointerfaces 170 (2018) 115–121, https://doi.org/10.1016/j.colsurfb.2018.06.003.

[10] D. Zeng, J. Zhao, K.H. Luk, S.T. Cheung, K.H. Wong, T. Chen, Potentiation of in vivo anticancer efficacy of selenium nanoparticles by mushroom polysaccharides surface decoration, J. Agric. Food Chem. 67 (2019) 2865–2876, https://doi.org/10.1021/acs.jafc.9b00193.

[11] M. Vahdati, T.T. Moghadam, Synthesis and characterization of selenium nanoparticles–lysozyme nanohybrid system with synergistic antibacterial properties, Sci. Rep. 10 (2020) 510, https://doi.org/10.1038/s41598-019-57333-7.

[12] K.V. Apryatina, E.I. Murach, S.V. Amarantov, E.I. Erlykina, V.S. Veselov, L. A. Smirnova, Synthesis of a bioactive composition of chitosan–selenium nanoparticles, Appl. Biochem. Microbiol. 58 (2022) 126–131, https://doi.org/10.1134/S0003683822020028.

[13] W. Liu, X. Li, Y.S. Wong, W. Zheng, Y. Zhang, W. Cao, T. Chen, Selenium nanoparticles as a carrier of 5-fluorouracil to achieve anticancer synergism, ACS Nano 6 (2012) 6578–6591, https://doi.org/10.1021/nn202452c.

[14] S. Menon, K.S.S. Devi, R. Santhiya, S. Rajeshkumar, V.S. Kumar, Selenium nanoparticles: a potent chemotherapeutic agent and its mechanism elucidation, Colloids Surf. B. Biointerfaces 170 (2018) 280–292, https://doi.org/10.1016/j.colsurfb.2018.06.006.

[15] T.M. Sakr, M. Korany, K.V. Katti, Selenium nanomaterials in biomedicine: an overview of new opportunities in nanomedicine of selenium, J. Drug Deliv. Sci. Technol. 46 (2018) 223–233, https://doi.org/10.1016/j.jddst.2018.05.023.

[16] V. Bartůněk, J. Junková, J. Šuman, K. Kolářová, S. Rimpelová, P. Ulbrich, Z. Sofer, Preparation of amorphous antimicrobial selenium nanoparticles stabilized by polysorbate 20, Mater. Lett. 152 (2015) 207–209, https://doi.org/10.1016/j.matlet.2015.03.092.

[17] S. Skalickova, V. Milosavljevic, K. Cihalova, P. Horky, L. Richtera, V. Adam, Selenium nanoparticles as a nutritional supplement, Nutrition 33 (2017) 83–90, https://doi.org/10.1016/j.nut.2016.05.001.

[18] B. Hosnedlova, M. Kepinska, S. Skalickova, C. Fernandez, B. Ruttkay-Nedecky, Q. Peng, M. Baron, M. Melcova, R. Opatrilova, J. Zidkova, G. Bjørklund, J. Sochor, R. Kizek, Nano-selenium and its nanomedicine applications: a critical review, Int. J. Nanomedicine 13 (2018) 2107–2128, https://doi.org/10.2147/IJN.S157541.

[19] Y. Wang, L.J. Feng, X.D. Sun, M. Zhang, J.L. Duan, F. Xiao, Y. Lin, F.P. Zhu, X. P. Kong, Z. Ding, X.Z. Yuan, Incorporation of selenium derived from nanoparticles into plant proteins in vivo, ACS Nano 17 (2023) 15847–15856, https://doi.org/10.1021/acsnano.3c03739.

[20] H. Shang, C. Ma, C. Li, Z. Cai, Y. Shen, L. Han, C. Wang, J. Tran, W.H. Elmer, J. C. White, B. Xing, Aloe vera extract gel-biosynthesized selenium nanoparticles enhance disease resistance in lettuce by modulating metabolite profile and endophyte composition, ACS Nano 17 (2023) 13672–13684, https://doi.org/10.1021/acsnano.3c02790.

[21] S.A. Wadhwani, U.U. Shedbalkar, R. Singh, B.A. Chopade, Biogenic selenium nanoparticles: current status and future prospects, Appl. Microbiol. Biotechnol. 100 (2016) 2555–2566, https://doi.org/10.1007/s00253-016-7300-7.

[22] G. Sharma, A. Kumar, S. Sharma, M. Naushad, R.P. Dwivedi, Z.A. AlOthman, G. T. Mola, Novel development of nanoparticles to bimetallic nanoparticles and their composites: a review, J. King Saud Univ. Sci. 31 (2019) 257–269, https://doi.org/10.1016/j.jksus.2017.06.012.

[23] H. Kaur, R. Mehta, S. Choudhury, M.A. Shah, D.K. Rathore, A. Mehta, Metallic nanoparticles in nanomedicine: Opportunities and challenges, in: M. Shukla, S. Ghoshal (Eds.), Nanomaterials in Diagnostic Tools and Devices, 1st ed., Academic Press, 2022, pp. 323–346.

[24] T.G. Moga, Counting on copper, Nat. Chem. 4 (2012) 334, https://doi.org/10.1038/nchem.1315.

[25] L.A. Silva, M.M. Victor, W.A. Lopes, S. Cunha, Cobre: produção industrial e aplicações, Quim. Nova 42 (2019) 1154–1161, https://doi.org/10.21577/0100-4042.20170439.

[26] M.I. Din, R. Rehan, Synthesis, characterization, and applications of copper nanoparticles, Anal. Lett. 50 (2017) 50–62, https://doi.org/10.1080/00032719.2016.1172081.

[27] M. Esmaeilirad, A. Kondori, B. Song, A.R. Belmonte, J. Wei, K. Kucuk, S. M. Khanvilkar, E. Efimoff, W. Chen, C.U. Segre, R. Shahbazian-Yassar, M. Asadi, Oxygen functionalized copper nanoparticles for solar-driven conversion of CO_2 to CH_4, ACS Nano 14 (2020) 2099–2108, https://doi.org/10.1021/acsnano.9b08792.

[28] M.L. Ermini, V. Voliani, Antimicrobial nano-agents: the copper age, ACS Nano 15 (2021) 6008–6029, https://doi.org/10.1021/acsnano.0c10756.

[29] J.K. Patra, G. Das, L.F. Fraceto, E.V.R. Campos, M. del Pilar Rodriguez-Torres, L. S. Acosta-Torres, L.A. Diaz-Torres, R. Grillo, M.K. Swamy, S. Sharma, S. B. Habtemariam, H. Shin, Nano based drug delivery systems: recent developments and future prospects, J. Nanobiotechnol. 16 (2018) 71, https://doi.org/10.1186/s12951-018-0392-8.

[30] S.S. Suri, H. Fenniri, B. Singh, Nanotechnology-based drug delivery systems, J. Occup. Med. Toxicol. 2 (2007) 16, https://doi.org/10.1186/1745-6673-2-16.

[31] J.M. Silva, M. Videira, R. Gaspar, V. Préat, H.F. Florindo, Biopolymer-based nanoparticles for topical drug delivery, Int. J. Pharm. 558 (2019) 328–343, https://doi.org/10.1016/j.ijpharm.2018.12.022.

[33] D. Dorfs, T. Härtling, K. Miszta, N.C. Bigall, M.R. Kim, A. Genovese, A. Falqui, M. Povia, L. Manna, Reversible tunability of the NIR valence band plasmon resonance in $cu_{2-x}Se$ nanocrystals, J. Am. Chem. Soc. 133 (2011) 11175–11180, https://doi.org/10.1021/ja2016284.

[34] F. Scotognella, G.D. Valle, A.R.S. Kandada, D. Dorfs, M. Zavelani-Rossi, M. Conforti, K. Miszta, A. Comin, K. Korobchevskaya, G. Lanzani, L. Manna, F. Tassone, Plasmon dynamics in colloidal $cu_{2-x}Se$ nanocrystals, Nano Lett. 11 (2011) 4711–4717, https://doi.org/10.1021/nl202390s.

[35] M. Nouri, H.R. Azimi, A.M. Saray, R. Yousefi, S-doping effects on optical properties and photocatalytic performance of cu_3se_2 nanoparticles under sunlight irradiation, Ceram. Int. 43 (2017) 14983–14988, https://doi.org/10.1016/j.ceramint.2017.08.018.

[36] L.J. Gong, Y.F. Li, H.Y. Zou, C.Z. Huang, Resonance light scattering technique for sensitive detection of heparin using plasmonic $cu_{2-x}Se$ nanoparticles, Talanta 216 (2020) 120967, https://doi.org/10.1016/j.talanta.2020.120967.

[37] I.G. Shitu, Z.A. Talib, J.L.Y. Chi, M.M.A. Kechick, H. Baqiah, Influence of tartaric acid concentration on structural and optical properties of CuSe nanoparticles synthesized via microwave assisted method, Results Phys. 17 (2020) 103041, https://doi.org/10.1016/j.rinp.2020.103041.

[38] K. Kaur, G. Rath, Formulation and evaluation of UV protective synbiotic skin care topical formulation, J. Cosmet. Laser Ther. 21 (2019) 332–342, https://doi.org/10.1080/14764172.2019.1658878.

[39] Y. Bai, Y. Wang, Y. Zhou, W. Li, W. Zheng, Modification and modulation of saccharides on elemental selenium nanoparticles in liquid phase, Mater. Lett. 62 (2008) 2311–2314, https://doi.org/10.1016/j.matlet.2007.11.098.

[40] A. Khalid, P.A. Tran, R. Norello, D.A. Simpson, A.J. O'Connor, S. Tomljenovic-Hanic, Intrinsic fluorescence of selenium nanoparticles for cellular imaging applications, Nanoscale 8 (2016) 3376–3385, https://doi.org/10.1039/C5NR08771F.

[41] B.S. Granja, J.R.H. Mendonça Filho, W.S. Oliveira, J.C.C. Santos, Exploring MBTH as spectrophotometric probe for total phenolic compounds determination in beverage samples, Anal. Methods 10 (2018) 2197–2204, https://doi.org/10.1039/c8ay00464a.

[42] W.S. Oliveira, J.C.C. Santos, Determination of total antioxidant capacity using thiamine as a natural fluorescent probe, J. Braz. Chem. Soc. 31 (2020) 2479–2490, https://doi.org/10.21577/0103-5053.20200123.

[43] J. Gubitosa, V. Rizzi, P. Fini, R. Del Sole, A. Lopedota, V. Laquintana, N. Denora, A. Agostiano, P. Cosma, Multifunctional green synthetized gold nanoparticles/chitosan/ellagic acid self-assembly: antioxidant, sun filter and tyrosinase-inhibitor properties, Mater. Sci. Eng. C 106 (2020) 110170, https://doi.org/10.1016/j.msec.2019.110170.

[44] J.V. Freitas, N.P. Lopes, L.R. Gaspar, Photostability evaluation of five UV-filters, trans-resveratrol and beta-carotene in sunscreens, Eur. J. Pharm. Sci. 78 (2015) 79–89, https://doi.org/10.1016/j.ejps.2015.07.004.

[45] J.S. Mansur, M.N.R. Breder, M.C.A. Mansur, R.D. Azulay, Determinação do fator de proteção solar por espectrofotometria, An. Bras. Dermatol. 61 (1986) 121–124.

[46] S. Boroumand, M. Safari, E. Shaabani, M. Shirzad, R. Faridi-Majidi, Selenium nanoparticles: synthesis, characterization and study of their cytotoxicity, antioxidant and antibacterial activity, Mater. Res. Express 6 (2019) 0850d8, https://doi.org/10.1088/2053-1591/ab2558.

[47] H. Cao, J. Xiao, H. Liu, Enhanced oxidase-like activity of selenium nanoparticles stabilized by chitosan and application in a facile colorimetric assay for mercury (II), Biochem. Eng. J. 152 (2019) 107384, https://doi.org/10.1016/j.bej.2019.107384.

[48] C.V. Restrepo, C.C. Villa, Synthesis of silver nanoparticles, influence of capping agents, and dependence on size and shape: a review, Environ. Nanotechnol. Monit. Manage. 15 (2021) 100428, https://doi.org/10.1016/j.enmm.2021.100428.

[49] T.G. Asere, Exploring Potential Environmental Applications of Selenium Nanoparticles, MSc, Thesis, Ghent University, Ghent, Belgium, 2013 https://libstore.ugent.be/fulltxt/RUG01/002/063/557/RUG01-002063557_2013_0001_AC.pdf (accessed 2024-07-01).

[50] B.P. Nenavathu, A. Sharma, R.K. Dutta, Se doped ZnO nanoparticles with improved catalytic activity in degradation of cholesterol, J. Water Environ. Nanotechnol. 3 (2018) 289–300, https://doi.org/10.22090/jwent.2018.04.002.

[51] S.F. Shayesteh, A.A. Dizgah, Effect of doping and annealing on the physical properties of ZnO:Mg nanoparticles, Pramana 81 (2013) 319–330, https://doi.org/10.1007/s12043-013-0562-z.

[52] V. Kumar, I. Rawal, V. Kumar, P.K. Goyal, Efficient UV photodetectors based on Ni-doped ZnS nanoparticles prepared by facial chemical reduction method, Phys. B 575 (2019) 411690, https://doi.org/10.1016/j.physb.2019.411690.

[53] M. El-Hagary, E.R. Shaaban, S.H. Moustafa, G.M.A. Gad, The particle size-dependent optical band gap and magnetic properties of Fe-doped CeO_2 nanoparticles, Solid State Sci. 91 (2019) 15–22, https://doi.org/10.1016/j.solidstatesciences.2019.03.005.

[54] W. Chen, Y. Li, S. Yang, L. Yue, Q. Jiang, W. Xia, Synthesis and antioxidant properties of chitosan and carboxymethyl chitosan-stabilized selenium nanoparticles, Carbohydr. Polym. 132 (2015) 574–581, https://doi.org/10.1016/j.carbpol.2015.06.064.

[55] S. Cavalu, I.V. Antoniac, L. Fritea, I.M. Mates, C. Milea, V. Laslo, S. Vicas, A. Mohan, Surface modifications of the titanium mesh for cranioplasty using selenium nanoparticles coating, J. Adhes. Sci. Technol. 32 (2018) 2509–2522, https://doi.org/10.1080/01694243.2018.1490067.

[56] J. Xiong, Y. Wang, Q. Xue, X. Wu, Synthesis of highly stable dispersions of nanosized copper particles using L-ascorbic acid, Green Chem. 13 (2011) 900–904, https://doi.org/10.1039/C0GC00772B.

[57] S.A. Khan, F. Noreen, S. Kanwal, A. Iqbal, G. Hussain, Green synthesis of ZnO and cu-doped ZnO nanoparticles from leaf extracts of *Abutilon indicum*, *Clerodendrum infortunatum*, *Clerodendrum inerme* and investigation of their biological and photocatalytic activities, Mater. Sci. Eng. C 82 (2018) 46–59, https://doi.org/10.1016/j.msec.2017.08.071.

[58] S.C. Mali, S. Raj, R. Trivedi, Biosynthesis of copper oxide nanoparticles using *Enicostemma axillare* (Lam.) leaf extract, Biochem. Biophys. Rep. 20 (2019) 100699, https://doi.org/10.1016/j.bbrep.2019.100699.

[59] S. Poulston, P.M. Parlett, P. Stone, M. Bowker, Surface oxidation and reduction of CuO and cu_2O studied using XPS and XAES, Surf. Interface Anal. 24 (1996) 811–820, https://doi.org/10.1002/(SICI)1096-9918(199611)24:12<811::AID-SIA191>3.0.CO;2-Z.

[60] C.H. Ramamurthy, K.S. Sampath, P. Arunkumar, M.S. Kumar, V. Sujatha, K. Premkumar, C. Thirunavukkarasu, Green synthesis and characterization of selenium nanoparticles and its augmented cytotoxicity with doxorubicin on cancer cells, Bioprocess Biosyst. Eng. 36 (2013) 1131–1139, https://doi.org/10.1007/s00449-012-0867-1.

[61] H. Kong, J. Yang, Y. Zhang, Y. Fang, K. Nishinari, G.O. Phillips, Synthesis and antioxidant properties of gum arabic-stabilized selenium nanoparticles, Int. J. Biol. Macromol. 65 (2014) 155–162, https://doi.org/10.1016/j.ijbiomac.2014.01.011.

[62] C. Zhang, X. Zhai, G. Zhao, F. Ren, X. Leng, Synthesis, characterization, and controlled release of selenium nanoparticles stabilized by chitosan of different molecular weights, Carbohydr. Polym. 134 (2015) 158–166, https://doi.org/10.1016/j.carbpol.2015.07.065.

[63] Y. Xiao, Q. Huang, Z. Zheng, H. Guan, S. Liu, Construction of a *Cordyceps sinensis* exopolysaccharide-conjugated selenium nanoparticles and enhancement of their antioxidant activities, Int. J. Biol. Macromol. 99 (2017) 483–491, https://doi.org/10.1016/j.ijbiomac.2017.03.016.

[64] A. Singh, A. Guleria, A. Kunwar, S. Neogy, M.C. Rath, Highly facile and rapid one-pot synthetic protocol for the formation of se nanoparticles at ambient conditions with controlled phase and morphology: role of starch and cytotoxic studies, Mater. Res. Express 6 (2019) 015029, https://doi.org/10.1088/2053-1591/aae615.

[65] T. Malinga, T. Kudanga, L.S. Mbatha, Stealth doxorubicin conjugated bimetallic selenium/silver nanoparticles for targeted cervical cancer therapy, Adv. Nat. Sci. Nanosci. Nanotechnol. 12 (2021) 045006, https://doi.org/10.1088/2043-6262/ac389c.

[66] B. Shan, Y. Zhao, Y. Li, H. Wang, R. Chen, M. Li, High-quality dual-plasmonic au@cu_{2-x}Se nanocrescents with precise cu_{2-x}Se domain size control and tunable optical properties in the second near-infrared biowindow, Chem. Mater. 31 (2019) 9875–9886, https://doi.org/10.1021/acs.chemmater.9b04100.

[67] W. Qiu, Y. Wang, M. Wang, J. Yan, Construction, stability, and enhanced antioxidant activity of pectin-decorated selenium nanoparticles, Colloids Surf. B. Biointerfaces 170 (2018) 692–700, https://doi.org/10.1016/j.colsurfb.2018.07.003.

[68] K. Kokila, N. Elavarasan, V. Sujatha, *Diospyros montana* leaf extract-mediated synthesis of selenium nanoparticles and their biological applications, New J. Chem. 41 (2017) 7481–7490, https://doi.org/10.1039/C7NJ01124E.

[69] B. El-Deeb, A. Al-Talhi, N. Mostafa, R. Abou-assy, Biological synthesis and structural characterization of selenium nanoparticles and assessment of their antimicrobial properties, Am. Sci. Res. J. Eng. Technol. Sci. 45 (2018) 135–170.

[70] A. Wolf, T. Härtling, D. Hinrichs, D. Dorfs, Synthesis of plasmonic cu_{2-x}Se@ZnS core@shell nanoparticles, Chemphyschem 17 (2016) 717–723, https://doi.org/10.1002/cphc.201500907.

[71] W.A. Lopes, M. Fascio, Esquema para interpretação de espectros de substâncias orgânicas na região do infravermelho, Quim Nova 27 (2004) 670–673, https://doi.org/10.1590/S0100-40422004000400025.

[72] A.F.S.A. Rahiman, S. Sethumanickam, Corrosion inhibition, adsorption and thermodynamic properties of poly(vinyl alcohol-cysteine) in molar HCl, Arabian J. Chem. 10 (2017) S3358–S3366, https://doi.org/10.1016/j.arabjc.2014.01.016.

[73] J. Yan, W. Qiu, Y. Wang, W. Wang, Y. Yang, H. Zhang, Fabrication and stabilization of biocompatible selenium nanoparticles by carboxylic curdlans with various molecular properties, Carbohydr. Polym. 179 (2018) 19–27, https://doi.org/10.1016/j.carbpol.2017.09.063.

[74] I. Khan, K. Saeed, I. Khan, Nanoparticles: properties, applications and toxicities, Arab. J. Chem. 12 (2019) 908–931, https://doi.org/10.1016/j.arabjc.2017.05.011.

[75] N.S. Dumore, M. Mukhopadhyay, Antioxidant properties of aqueous selenium nanoparticles (ASeNPs) and its catalyst activity for 1,1-diphenyl-2-picrylhydrazyl (DPPH) reduction, J. Mol. Struct. 1205 (2020) 127637, https://doi.org/10.1016/j.molstruc.2019.127637.

[76] N. Shahabadi, S. Zendehcheshma, F. Khademic, Selenium nanoparticles: synthesis, in vitro cytotoxicity, antioxidant activity and interaction studies with ct-DNA and HSA, HHb and Cyt c serum proteins, Biotechnol. Rep. 30 (2021) e00615, https://doi.org/10.1016/j.btre.2021.e00615.

[77] P. Park, J. Je, S. Kim, Free radical scavenging activities of differently deacetylated chitosans using an ESR spectrometer, Carbohydr. Polym. 55 (2004) 17–22, https://doi.org/10.1016/j.carbpol.2003.05.002.

[78] G.J. Beckett, J.R. Arthur, Selenium and endocrine systems, J. Endocrinol. 184 (2005) 455–465, https://doi.org/10.1677/joe.1.05971.

[79] C. Mellinas, A. Jiménez, M.D.C. Garrigós, Microwave-assisted green synthesis and antioxidant activity of selenium nanoparticles using *Theobroma cacao* L. bean shell extract, Molecules 24 (2019) 4048, https://doi.org/10.3390/molecules24224048.

[80] Z. Huang, B.J. Guo, R.N.S. Wong, Y. Jiang, Characterization and antioxidant activity of selenium-containing phycocyanin isolated from *Spirulina platensis*, Food Chem. 100 (2007) 1137–1143, https://doi.org/10.1016/j.foodchem.2005.11.023.

[81] S.P. Mohanty, N. Mishra, B. Singhal, D. Singh, R. Srivastava, M.K. Singh, Key physicochemical parameters influencing the fate and toxicity of engineered nanomaterials: implications for biomedical applications, Mater. Sci. Eng. C 108 (2020) 110411, https://doi.org/10.1016/j.msec.2019.110411.

[82] D. Medina Cruz, E. Mostafavi, A. Vernet-Crua, C.P. O'Connell, H. Barabadi, S. Mobini, J.L. Cholula-Diaz, G. Guisbiers, J.M. Garcia-Martin, T.J. Webster, Green nanotechnology and nanoselenium for biomedical applications, in: T.J. Webster (Ed.), Nanomedicine, 2nd ed, Woodhead Publishing Series in Biomaterials, 2023, pp. 339–380.

[83] ANVISA (National Sanitary Surveillance Agency), Brazilian Resolution RDC No. 629, 2022 https://www.in.gov.br/web/dou/-/resolucao-rdc-n-629-de-10-de-marco-de-2022-386099957 (accessed 2024-07-19).

[84] D.G. Yeager, H.W. Lim, What's new in photoprotection: a review of new concepts and controversies, Dermatol. Clin. 37 (2019) 149–157, https://doi.org/10.1016/j.det.2018.11.003.

[85] V.P. Baillo, A.C. Lima, Nanotecnologia aplicada à fotoproteção, Rev. Bras. Farm. 93 (2012) 271–278.

[86] G.M.G. Saucedo, R.S. Vallejo, J.C.M. Giménez, Effects of solar radiation and an update on photoprotection, An. Esp. Pediatr. 92 (377) (2020) e1–377.e9, https://doi.org/10.1016/j.anpede.2020.04.003.

[87] R. Rajamohan, P. Muthuraja, C. Govindasamy, S.A. Subramanian, S.J. Kim, M. M. Krishnan, K. Murugavel, Y.R. Lee, Enhanced photostability and biocompatibility of sunscreen formulation of 2-phenylbenzimidazole-5-sulfonic acid with methyl-

beta-cyclodextrin, J. Mol. Liq. 390 (2023) 123013, https://doi.org/10.1016/j.molliq.2023.123013.
[88] F.A.S. Addor, C.B. Barcaui, E.E. Gomes, O. Lupi, C.R. Marçon, H.A. Miot, Sunscreen lotions in the dermatological prescription: review of concepts and controversies, An. Bras. Dermatol. 97 (2022) 204–222, https://doi.org/10.1016/j.abd.2021.05.012.
[89] R.C. Romanhole, J.A. Ataide, L.C. Cefali, P. Moriel, P.G. Mazzola, Photostability study of commercial sunscreens submitted to artificial UV irradiation and/or fluorescent radiation, J. Photochem. Photobiol. B 162 (2016) 45–49, https://doi.org/10.1016/j.jphotobiol.2016.06.011.
[90] L. Yuan, S. Li, D. Huo, W. Zhou, X. Wang, D. Bai, J. Hu, Studies on the preparation and photostability of avobenzone and (2-hydroxy)propyl-β-cyclodextrin inclusion complex, J. Photochem. Photobiol. A 369 (2019) 174–180, https://doi.org/10.1016/j.jphotochem.2018.09.036.
[91] R. Jansen, U. Osterwalder, S.Q. Wang, M. Burnett, H.W. Lim, Photoprotection: part II. Sunscreen: development, efficacy, and controversies, J. Am. Acad. Dermatol. 69 (2013) 867–881, https://doi.org/10.1016/j.jaad.2013.08.022.

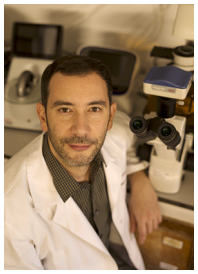

Jose L. Luque-Garcia is currently a Full Professor at Complutense University of Madrid, Spain. He received his PhD degree in Analytical Chemistry from the University of Cordoba, Spain in 2003. His main research interests include design of novel nanomaterials for biomedical applications, and use and development of bioanalytical methods, with special emphasis on omics technologies.

Daniela S. Anunciação is currently a Professor at Federal University of Alagoas, Brazil. She received her PhD degree in Analytical Chemistry from the Federal University of Bahia, Brazil in 20112. Her main research interests focus on nanotechnology applied to sustainable agriculture, environmental chemistry, development of bioanalytical methods, and technological innovation for low-cost and field-deployable analytical solutions.